A Probabilistic Model to Evaluate Options for Mitigating Induced Seismic Risk

Jan van Elk,[a] M.EERI, Stephen J Bourne,[b] Steve J Oates,[c] Julian J Bommer,[d] M.EERI, Rui Pinho,[e] M.EERI, and Helen Crowley,[f] M.EERI

Common responses to induced seismicity are based on control of the anthropogenic activity causing the earthquakes, like fluid injection or withdrawal, in order to limit either the magnitudes of the events or the level of ground motion to within established thresholds. An alternative risk mitigation option is seismic retrofitting of the more vulnerable buildings potentially exposed to the ground shaking in order to reduce the risk to acceptable levels. Optimal mitigation strategies may combine both production control and structural strengthening, for which a probabilistic risk model is required that can estimate the change in hazard due to production or injection variations and the changes in fragility resulting from structural interventions. Such a risk model has been developed for the Groningen gas field in the Netherlands. The framework for this risk model to inform decision-making regarding mitigation strategies can be adapted to other cases of anthropogenically-induced seismicity.

INTRODUCTION

In recent years the societal impact of induced earthquakes resulting from human activities—especially the extraction or injection of fluids—has received increasing attention. This has largely been due to an increase in the public awareness and concern, as well as regulatory response to what is a risk induced by human activity rather than one arising from a natural hazard.

Earthquake engineering has generally focused on the provision of seismic resistance to the built environment to protect society from the effects of naturally occurring tectonic

[a] Nederlandse Aardolie Maatschappij B.V. (NAM), Schepersmaat 2, 9405 TA Assen, The Netherlands
[b] Shell Global Solutions International B.V., Grasweg 31, 1031HW Amsterdam, The Netherlands
[c] Shell Global Solutions International B.V., Kessler Park 1, 2288 GS Rijswijk, The Netherlands
[d] Civil & Environmental Engineering, Imperial College London, London SW7 2AZ, U.K.
[e] Civil Engineering & Architecture, University of Pavia, via Ferrata 1, Pavia, Italy
[f] Seismic Risk Consultant, Pavia, Italy

earthquakes; the hazard in terms of ground shaking is quantified to inform design decisions but cannot be modified. The response to induced seismicity, however, has tended to focus on the potential for controlling the seismicity—and therefore the seismic hazard—through modification (or suspension) of the human activity causing the earthquakes. Hence there has been a great emphasis on 'traffic light systems', especially for those operations associated with high-pressure injection of liquids such as enhanced geothermal systems (Majer et al. 2012) and waste water disposal (Zoback 2012). The efficacy of such control schemes depends in part on a rapid response of the system to changes in withdrawal or injection operations. Moreover, in geothermal projects, for example, the largest induced earthquakes have tended to occur after shut-in of injection operations (Majer et al. 2007).

For conventional natural gas production in a field as large as Groningen, uncertainty regarding the response to short-term production changes means that production measures in combination with selective building strengthening should be considered as a more effective risk mitigation strategy. Nonetheless, reduction of gas production levels is an option for limiting the induced earthquake activity and the consequent hazard and risk. However, it is not the only option to reduce seismic risk since the principles of earthquake engineering can also be applied to induced seismicity as they have been applied to natural earthquakes for several decades. Some studies, such as Douglas and Aochi (2014) and Mignan et al. (2015), have addressed the risk due to induced earthquakes, but the proposed responses are still focused on control of the seismic hazard.

While options for controlling the driving force behind induced seismicity should clearly be considered in any risk management scheme, approaches focusing on hazard reduction do not need to be the unique focus since traditional earthquake engineering can be applied to reduce fragility as an alternative risk mitigation response (Bommer et al. 2015). Development of a quantitative probabilistic risk model that predicts the change in hazard resulting from modifications to production and the change in fragility resulting from structural upgrading can serve as the basis for designing a set of risk mitigation strategies. Even if the focus remains primarily on hazard control, a probabilistic risk model considering the distribution and characteristics of the exposure provides a more complete basis for determining acceptable production levels based on safety norms which are provided by society.

This paper presents a probabilistic hazard and risk model that has been developed to inform decision-making regarding mitigation options in the Groningen gas field in the

Netherlands, where production-induced earthquakes have raised serious societal concerns. The hazard and risk model development has been supported by extensive new data collection in order to calibrate the model components to local conditions, but attention has also been paid to ensuring adequate capture of the inevitable uncertainty associated with modeling the effects of potential larger-magnitude earthquakes. The presentation of the complete risk model would clearly exceed the available length for a single journal article; this paper is the culmination of a series of papers in which individual elements of the risk model have been previously presented in the open literature (namely Bourne et al. 2015; Bourne et al. 2018; Bommer et al. 2017a; Crowley et al. 2017; Crowley et al. 2018). Key features of the model elements are summarized herein and references provided for the reader interested in greater detail. The purpose of the present paper is to show how these model elements are combined into a comprehensive risk model (including the rigorous quality assurance procedures applied) and to demonstrate its capabilities in terms of quantifying the risk reductions achievable through different mitigation measures. While the risk estimates for the Groningen field will be of interest to some readers, the primary purpose of the paper is to present the general framework that can be adapted to other cases of induced seismicity. To our knowledge, this is the first presentation of a complete risk model for induced earthquakes.

In closing this introduction, it is important to emphasize that decisions regarding risk mitigation strategies will also be influenced by many other considerations, including community perception of risk (Slovic 2000, 2010) and recurring building damage, potential for damage to heritage buildings, security of supply to the dedicated gas market for Groningen-quality gas consisting mainly of households and small industry, regulatory control, social trust in risk management (Cvetkovich and Löfstedt 1999, Siegrist et al. 2010), economics, and international energy security issues. Such contextual factors, both in Groningen and in general, are beyond the scope of this article. However, regardless of the specific details and sensitivities of any specific case of induced or triggered seismicity associated with human activities, a probabilistic risk model contributes to informed and balanced decision making.

IMPLEMENTATION OF THE RISK MODEL

This section introduces the main elements of the risk model for the quantitative estimation of seismic risk metrics in the Groningen field. Each of these elements will then be described in more detail in subsequent sections of this paper.

RISK METRICS

In early 2015, an advisory committee, Commissie Meijdam, was established to advise on risk policy related to Groningen earthquakes, including the selection of risk metrics. The first recommendation of this committee was that a local personal risk (LPR) metric, defined as the annual probability of fatality for a hypothetical person who is continuously present without protection inside a building, should be evaluated for all buildings within the assessment area. The capability to estimate this risk metric was thus the main priority for the development of the risk model, but a number of other risk metrics are also being implemented and investigated. These include group or societal risk presented through so-called F-N curves for both fatalities and damaged buildings (i.e., the frequency of occurrence F, of at least N fatalities or damaged buildings in a single event) and average annual loss due to repair of damage.

RISK SIMULATIONS

The risk model is evaluated by Monte-Carlo sampling of the aleatory variability within the causal sequence of conditional probability models (Figure 1), building on the hazard model by Bourne et al. (2015).

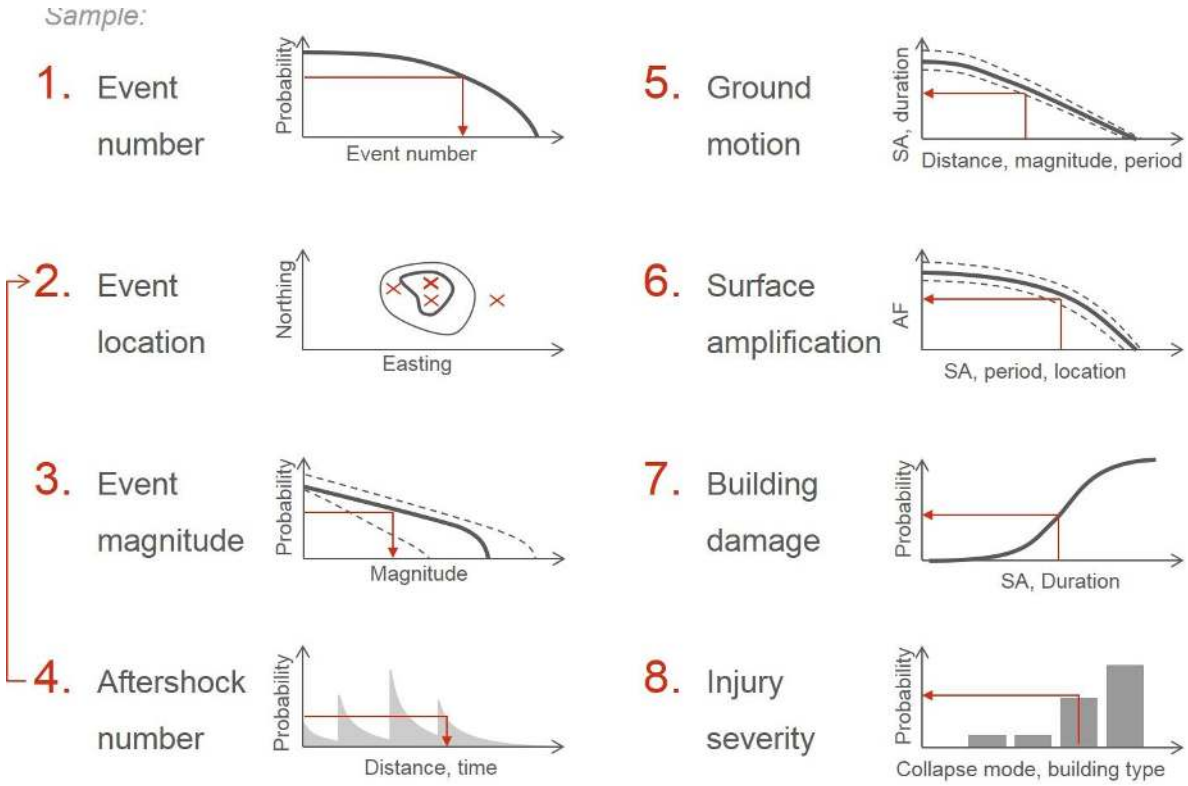

Figure 1. Schematic diagram of risk calculation process when focused on casualty estimation.

For a given risk assessment period and a given gas production scenario, the spatial-temporal development of reservoir pore pressure changes is forecast by using the reservoir fluid flow simulation model. Given these pressure changes, the seismological model forecasts probability distributions for the total number of induced earthquakes, the epicentral locations, origin times, and magnitudes, including contributions from aftershocks. Sampling these earthquake distributions creates a single simulated earthquake catalog.

Given this simulated catalog, the ground motion model forecasts the probability distribution of base rock motions and near-surface amplifications for every simulated earthquake exceeding a given threshold and for every surface location within a dense surface grid of observation points. Sampling these ground motion distributions creates a single catalog of simulated ground motions.

For the primary risk metric of local personal risk, spatial correlation is unimportant but for aggregate measures, such as group risk, the influence of spatial correlation of ground motions can be very important. In the current model, rules are imposed for sampling the variability distributions in order to produce near-perfect correlation of the ground motions at all grid points within a site response zone. The resulting distribution of highly-correlated ground motions within each zone and no correlation between zones provides a good first-order approximation to a more realistic model for the variation of spatial correlation with separation distance (Stafford et al., 2018).

Given the simulated catalog of ground motions, the fragility model forecasts the probability distribution of building damage states for each recognized structural system for each ground motion event at each observation point. Sampling these probability distributions for each exposed building yields a catalog of damaged buildings.

Given this catalog of damaged buildings, the fatality model forecasts the probability distribution of loss of life for each exposed building and collapse mechanism. Sampling these consequence distributions creates a single catalog of simulated fatality probabilities. Repeating this sampling process a sufficiently large number of times yields a collection of simulated catalogs that closely approximate the fatality probability distribution. Risk metrics that summarize this distribution are then readily computable.

INDUCED EARTHQUAKES IN THE GRONINGEN FIELD

The Groningen gas field (Figure 2), was discovered in 1959. Initially, gas reserves were estimated at some 2900 billion cubic meters (bcm).

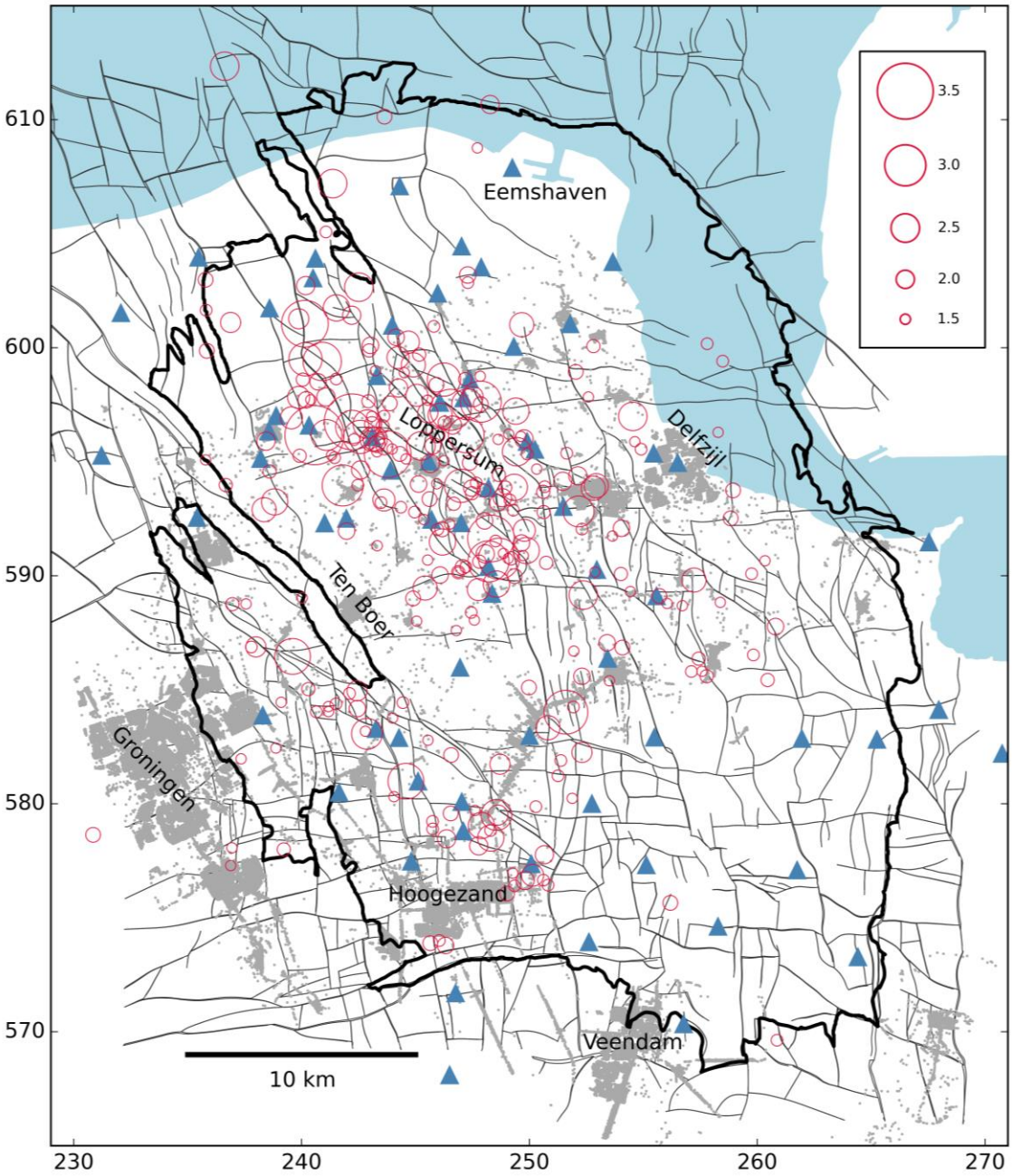

Figure 2. Location map with earthquake epicenters (all events with $M_L \geq 1.5$ between 1995 and 2017) shown as red circles (local magnitudes in legend) from the KNMI catalog, overlain on a base map showing the Groningen field outline, mapped geological faults, seismometer stations (blue triangles) and building locations (gray dots); major urban settlements are labeled. Coordinates are in 1000s of meters in the Dutch RD system.

Gas production started in 1963 and a peak annual production rate of 88 bcm was reached in 1976. The remaining gas volume that could potentially still be produced is estimated at

800 bcm. Between 1995 and 2014, annual production varied with demand between 23 and 54 bcm, but has since been successively cut on the instruction of the Government, in response to growing concerns about the induced earthquakes. Production from the center of the field started being reduced in January 2014; total annual volumes were 53.87 bcm (2013), 42.41 bcm (2014), 28.10 bcm (2015), 27.59 bcm (2016) and 23.58 bcm (2017).

The Groningen reservoir consists of high quality reservoir sandstone with a thick gas column. The field is heavily faulted with more than 1,500 faults identified on the 3D seismic data. The field is produced from 20 production clusters and two satellite clusters. At the production clusters, the gas is compressed and processed (removal of small amounts of produced water and condensate). The clusters are connected via a pipeline network through which gas is supplied to the national grid.

The first earthquake recorded in the north of the Netherlands was in December 1986 and since 1993 it has been accepted that seismicity in the area is induced by production from the northern gas fields – Groningen (Figure 2) and others. The 1986 event occurred close to the Assen field whereas the first production-related earthquake detected within the Groningen field was in 1991. To date there have been 17 Richter local magnitude (M_L) $\geq$3.0 earthquakes in the northern Netherlands: nine in the Groningen field, four in the Bergermeer field and three in the Roswinkel field (KNMI 2017).

The triggering of tectonic events is considered to be very unlikely, given the very low level of natural seismicity as revealed by historical and instrumental records, which would suggest that the crust in this region is not critically stressed. Houtgast's (1992) catalog of historical earthquakes in the Netherlands lists only one candidate event – on 28 January 1262 – in the north of the Netherlands prior to the first instrumentally-recorded event in 1986. The seismological service of KNMI, however, now interprets the effects attributed to an earthquake in the 13th century as being of meteorological origin (B. Dost, *personal communication*, 2017).

In August 2012 the area's largest induced earthquake occurred close to the village of Huizinge, in the center of the Groningen field. This M_L 3.6 event was widely felt and led to numerous claims for minor damage to buildings and long-running public and political debate. Furthermore, the number of earthquakes per unit gas production was seen to be increasing with cumulative gas production (Bourne and Oates, 2017). These considerations have driven the densification of the earthquake monitoring network over the field as described below.

DATA ACQUISITION FOR FIELD CHARACTERIZATION

In order to provide the best possible constraint on the hazard and risk estimates for the Groningen region, the production and exploration company Nederlandse Aardolie Maatschappij B.V. (NAM) has invested in a comprehensive collection of new data to characterize both the subsurface of the Groningen field, the near-surface conditions, the nature of shaking caused by induced earthquakes, and the exposed building stock. The following sections summarize these data collection activities.

For completeness, however, it is noted that, in addition to the data collection activities described below, a gravity survey was carried out to better calibrate gas and water movement in the reservoir, a fiber-optic cable was installed over the reservoir section to measure compaction and a core has been taken over the reservoir section to do compaction and rupture experiments; the latter refer to lab tests whereby rock specimens are moved alongside each other, under controlled pressure and temperature conditions, while friction is measured (Spiers et al. 2017, Hunfeld et al. 2017, Pijnenburg et al. 2018).

SEISMOLOGICAL AND STRONG-MOTION MONITORING

KNMI, the Royal Netherlands Meteorological Institute, monitors seismicity in the Netherlands. Following the onset of detectable seismicity in the north of the Netherlands, a near-surface seismic monitoring network was deployed over the NE Netherlands by KNMI and by 1995 was fully operational. This network, with additions in 2009 and 2010, was relatively sparse with six stations over or close to the Groningen field, each with three-component geophones deployed at four depths in 120 to 300 m deep boreholes. The magnitude of completeness for events located by this array is taken to be M_L 1.5, starting in April 1995 (Dost et al. 2012). A small number of surface accelerographs was also deployed in the field, which recorded several earthquakes including the 2012 Huizinge M_L 3.6 event. The largest horizontal component of acceleration recorded in the event was 0.08g, which remained the maximum PGA in the Groningen database until exceeded by a peak of 0.11g recorded by a much denser network during an earthquake of M_L 3.4 on 8 January 2018.

The public and political response to the 2012 Huizinge earthquake and the escalation of seismic activity within the field necessitated more detailed monitoring to better characterize the induced seismicity. It was decided to increase the density of the earthquake monitoring network over the field to lower the detection and location thresholds and improve location

accuracy (Dost et al. 2017). Between 2014 and 2016 some 70 stations were added with an average spacing of between 4 and 5 km. The completeness of the expanded network is close to M_L 0.5, epicenters are located with an accuracy of 100 to 300 m and depths can be estimated for most events with an accuracy of about 300 m. However, in routine locations, KNMI generally constrains the focal depths to 3000 m, which is the approximate average depth of the gas reservoir (Figure 3). With the exception of a few small-magnitude events, most earthquake hypocenters have been placed within the Rotliegend sand layer that contains the reservoir and is between 200 and 300 m thick over most of the field (Spetzler and Dost 2017). For events of M_L 2.5 and larger, M_L values determined by KNMI are, on average, equivalent to moment magnitudes (Dost et al. 2018). The recordings obtained from the accelerograph and geophone networks have provided the basis for the derivation of the ground-motion prediction model.

To complement the near-surface network, geophone strings were deployed in wells, some 3 km below the surface in the Rotliegend reservoir. Placing geophones at reservoir level, close to the most seismically active part of the field, enables detection of many of the micro-earthquakes not detectable at surface. Additionally, some 300 accelerometers have been deployed close to foundation levels in public buildings and private houses in the region (Borsje et al. 2016).

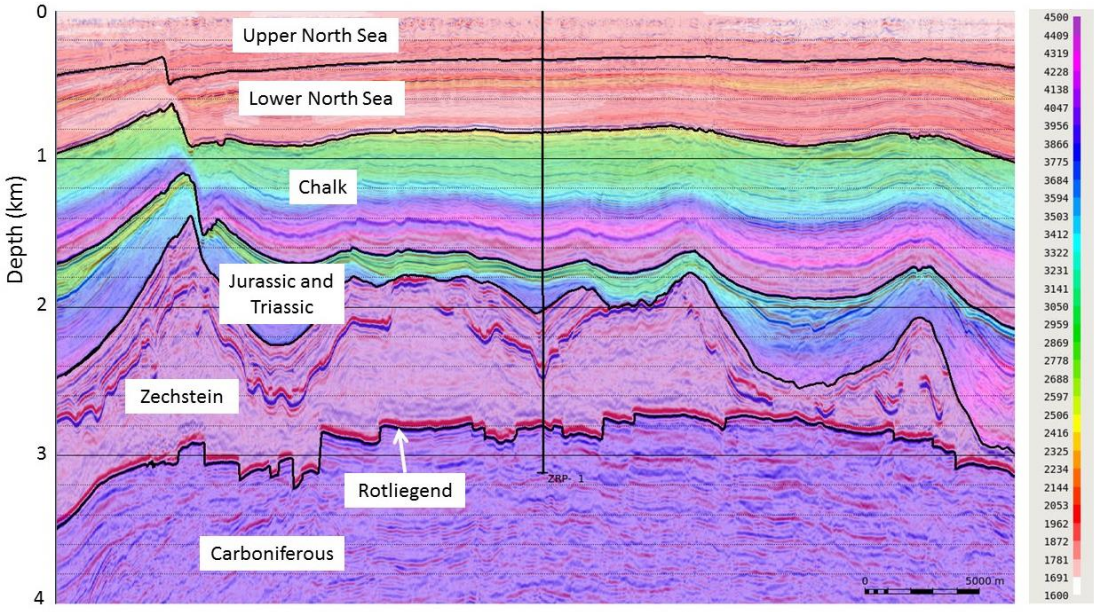

Figure 3. East-west cross-section through the northern part of the Groningen field, intersecting the deep ZRP1 well, indicating the main stratigraphic intervals marked by black lines; the gas reservoir is in the Rotliegend Slochteren sandstone. Colors indicate P-wave velocities in m/s, shown in the legend (ranging from 1,600 to 4,500 m/s). Source: NAM.

GEODETIC MONITORING

Groningen gas production lowers the pressure of gas contained within the reservoir pore-space causing the reservoir to compact and the overlying Earth's surface to subside. Repeated geodetic observations measure this surface subsidence allowing us to image the spatial-temporal evolution of reservoir compaction. This reservoir compaction history loads the pre-existing intra-reservoir faults and governs their accumulation of stress and induced seismicity. Utilizing this information, we reduce uncertainty about the spatial-temporal evolution of induced seismicity with decreasing gas pressure within the seismological model. Three independent geodetic monitoring systems have measured the spatial-temporal development of these induced surface displacements with a precision of 1-2 mm/year. First, optical-levelling surveys began in 1964 and thereafter were repeated about every 5 years to yield estimates of surface elevation changes up to about 8 mm/year (Bourne et al. 2014). Second, space-borne interferometric synthetic aperture radar (InSAR) monitoring began in 1995 (Ketelaar 2008, 2009) to measure the monthly time series of line-of-sight displacements. Third, a sparse, field-wide network of 13 permanent Global Positioning System (GPS) sensors began in 2014 to measure the daily time series of three-dimensional vector displacements. The surface subsidence in the field resulting from the reservoir compaction is shown in Figure 4. Recently, monuments have been installed with a satellite reflector, levelling marker and GPS station to allow better reconciliation of these three measurement techniques.

VELOCITY PROFILES AND NEAR-SURFACE SOIL CHARACTERISTICS

A key element of the risk model is ground-motion predictions that account for the variations in near-surface shear-wave velocity (V_S) profiles and nonlinear soil properties across the field. The base of the Lower North Sea formation at a depth of about 800 m (Figure 3) is treated as the reference rock horizon, with site response analyses conducted to determine the amplification factors of the overlying layers (Rodriguez-Marek et al. 2017). Kruiver et al. (2017) describe in detail the construction of the V_S profiles for the entire gas field using a geological model for the uppermost 50 m, sonic logs for the deeper profiles and surface-wave inversions for the intervening depth range. The shallow portion of the V_S profiles have been validated through *in situ* measurements at the permanent KNMI accelerograph stations (Noorlandt et al. 2018) and inversion of geophone records from the

borehole stations (Spica et al. 2018). The time-averaged 30-meter V_S values (V_{S30}) across the field range between 156 and 269 m/s.

Low-strain damping of the near-surface layers have been estimated from borehole geophone recordings and used to adjust standard damping *vs*. shear strain curves for soils (Rodriguez-Marek et al. 2017). Peats are present in much of the field area and NAM has commissioned a campaign of undisturbed sampling and laboratory testing of the shallow peats in order to estimate their dynamic characteristics.

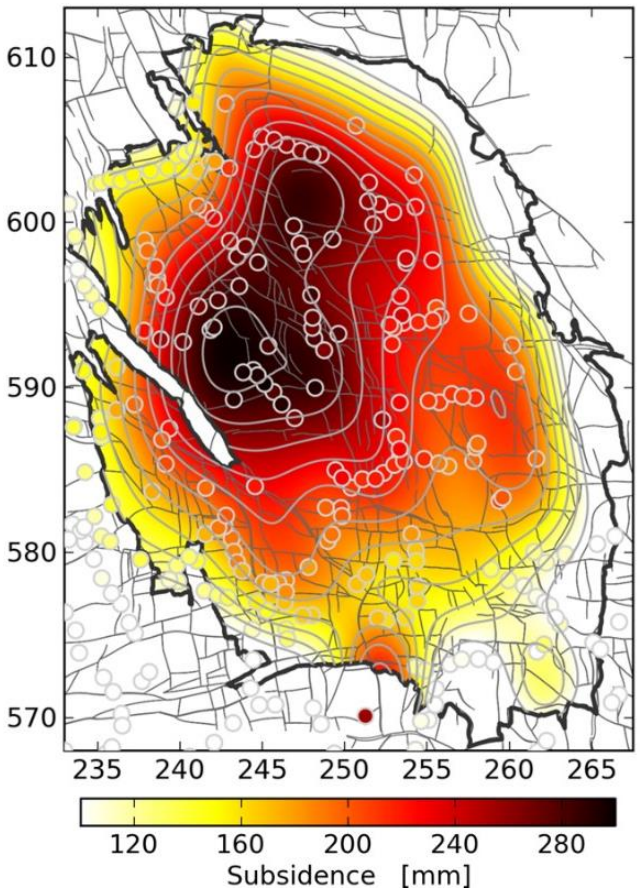

Figure 4. The network of optical levelling benchmarks (circles) and the surface subsidence measured by this network from 1972 to 2011 in relation to the outline of the Groningen gas field (black polygon) and mapped reservoir faults (black lines)

BUILDING AND POPULATION DATABASE

Each building within the assessment area, a 5 km buffer around the field outline (as shown in Figure 2), has been uniquely identified using the governmental BAG (Basisregistratie Adressen en Gebouwen) dataset, which also provides the building coordinates, year of construction, footprint area, useable floor area and number of addresses (i.e., each geographic location made up by street name, house number, letter, postal code and

town) within each of the approximately 260,000 buildings (Arup 2017a). The use of each building is also available from the BAG dataset, and this is further verified using a number of additional datasets including the national registries of schools (Dienst Uitvoering Onderwijs), of public health buildings (Nationale Atlas Volksgezondheid), and national monuments (Rijksdienst voor het Cultureel Erfgoed). The height of the buildings has been estimated from a detailed height model of the Netherlands obtained from laser altimetry (Actueel Hoogtebestand Nederland).

For a large number of buildings within the center of the field, GIS spatial analysis techniques have also been used to extract parameters such as roof span length, roof steepness, and adjacency, which are used, together with the geometrical and height data, to help classify the structural layout of each building. The validation of this approach is discussed further in Arup (2017a). Examples of structural layouts include houses, barns, warehouses, apartment blocks, and sheds. The structural layout, together with the age of the building, is then used to infer the structural system, discussed further in the Exposure Model section. In order to better understand the range of structural systems used to construct buildings within the region, a large number of Extensive Visual Screening (EVS) inspections have been carried out and structural drawings of many buildings have been obtained from local municipalities.

The data related to the population living and working within the region has been obtained from a number of sources including the Central Statistical Office of the Netherlands (CBS) and the Nationaal Coördinator Groningen (NCG). The distribution of the population between buildings with different usage categories during the day and night has been estimated using data from the Dutch Ministry of Education (OCW), the National Register of Childcare and Children's Playgrounds, and the Social Cultural Planning Bureau (who produce reports on how people in the Netherlands spend their time). Of the 260,000 buildings in the region, only around 150,000 are populated as many of the buildings in the original database refer to small sheds that are not regularly occupied. The population data indicates that there are between 425,000 and 470,000 people living and/or working within the region during the night and day, respectively.

STRUCTURAL TESTING AND ANALYSES

The construction culture and practice in the, until recently aseismic, Groningen region (e.g., Figure 5) is understandably and naturally distinct from that typically found in areas of the world that have a long history of damaging earthquakes. As such, neither experimental

data nor verified numerical models for the characterization of the seismic response of these types of structures were available at the start of the current endeavor. Consequently, an extensive structural testing campaign and numerical validation and calibration program had to be deployed in order to obtain data to constrain the derivation of the fragility models, as described in the following.

To start with, material characterization efforts were first initiated, leading to the *in situ* destructive and non-destructive testing of several tens of (mainly masonry) samples, the results of which were then compared with companion material tests on more than 200 laboratory specimens featuring calcium silicate bricks, clay bricks, mortar, concrete and steel materials. This effort allowed the development of a database of typical material mechanical properties for the region, to be used in the subsequent structural modeling activities (e.g., Graziotti et al. 2016a, 2018b).

Cyclic and dynamic (shake-table) testing on a large number of structural components such as masonry panels (e.g., Graziotti et al. 2016b, 2018a) and reinforced concrete precast panels and connections (e.g., Brunesi and Nascimbene, 2017) then followed, with a view to gather data necessary for the initial efforts on verification and calibration of numerical models (Figure 6).

Figure 5. Examples of reinforced concrete construction (with masonry cladding) in the Groningen region: cast-in-place (above), precast (below)

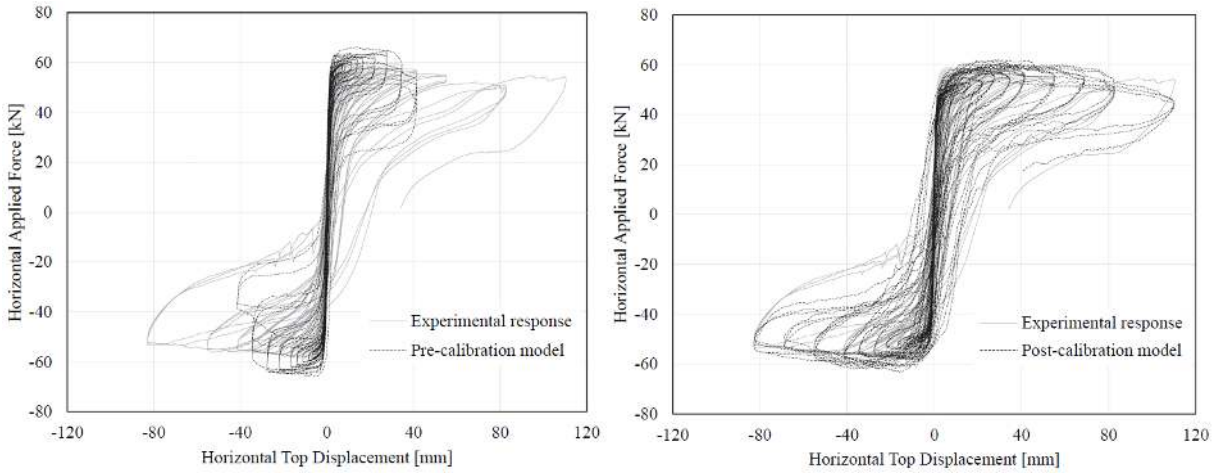

Figure 6. Comparisons between the recorded response of a calcium-silicate wall specimen tested under cyclic loading and the corresponding numerical prediction (i.e., before model calibration) and post-diction (i.e., after model calibration) (Malomo et al. 2017).

Finally, the cyclic and dynamic testing of nine full-scale specimens was performed, involving four cavity wall terraced houses (e.g., Figure 7), two solid wall detached houses, three RC cast-in-place and precast wall-slab-wall frames (e.g., Graziotti et al. 2017a; Kallioras et al. 2018; Brunesi et al. 2018a, 2018b). Both for reasons of shake-table control as well as to monitor damage/limit states evolution, these test specimens are subjected to earthquake loading of increasing intensity, all the way up to either a full- or a near-collapse response condition.

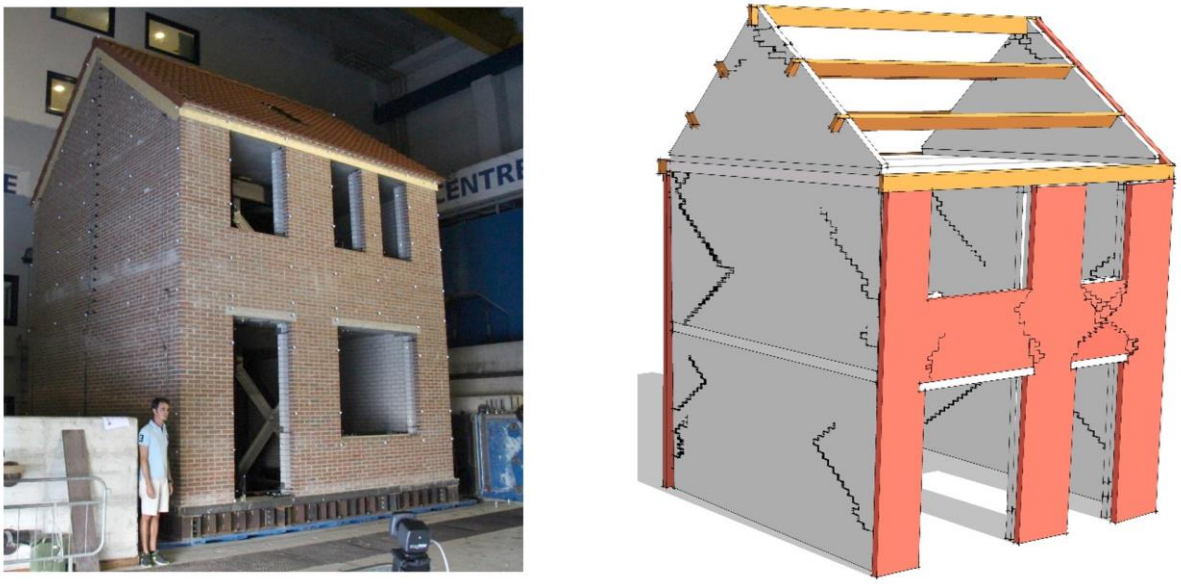

Figure 7. Left: Terraced house full-scale specimen on shake-table; Right: observed damage pattern (Graziotti et al. 2017a)

For each of these full-scale tests, a number of structural modeling teams, each using different modeling approaches, were invited to carry out, first, blind-predictions of the tests results, and then calibrated "post-dictions" (e.g., Arup et al. 2015; 2016; 2017). This cross-modeling validation exercise served to calibrate the structural analysis software tools that are being employed in the modeling of a large number of actual buildings representative of the different building typologies present in the region (Arup 2017b, Mosayk 2017). The results of the modeling are then used in the derivation of fragility functions, as described in subsequent sections of this paper.

ELEMENTS OF THE GRONINGEN RISK MODEL

This section describes the development of the individual elements of the risk model (presented previously in Figure 1), forming a chain from gas production scenarios through induced events, shaking scenarios, building response, and consequences (loss of life) for building inhabitants. In each case, the models are validated and calibrated using all available data from the field while also capturing the remaining epistemic uncertainty that is not removed through the additional data collection.

GAS PRODUCTION SCENARIOS

Gas is produced from some 200 wells grouped across 20 cluster locations. The production capacity of the wells at these locations is limited both by declining reservoir pressure and the capacity of the installed compressors.

The first step in the process of hazard and risk forecasting is modeling of the reservoir fluid flow for a range of anticipated future production scenarios. The underlying reservoir model is history-matched by imposing the historical gas production data from the wells at the clusters against the reservoir pore-pressure measured by in-well sensors, production of formation water, gravity measurements at surface and compaction from inversion of the subsidence measured at surface (van Oeveren et al. 2017). The pressure depletion maps generated by these simulations of future production are then used to generate reservoir compaction maps, according to a linear compaction model estimated from geodetic monitoring data, which in turn will be the primary input to the seismological model described below. Hazard and risk forecasts can be run for any gas production scenario as defined by a total annual production rate and the distribution of this production over the production clusters withdrawing gas from the different areas of the field.

Since induced seismicity over the Groningen field is ultimately caused by reservoir pressure depletion, the seismic hazard should change in response to changes in the volume and spatial distribution of gas production. Indeed, the operator was tasked by the authorities to investigate whether an alternative distribution of production could reduce the seismic hazard or risk. The scope to redistribute the production is, however, limited both by regulatory constraints and by constraints in the production system itself.

The production reductions of around 90% for the five production clusters near Loppersum were imposed in January 2014 and were initially successful in temporarily arresting the pressure decline – and hence compaction – in that region. However, the imbalance in offtake rates has resulted in a pressure gradient driving flow of gas from this region in the northwest of the field to the southeast of the field. With continued production in the south and east of the field, the pressure decline in the Loppersum area will revert to the field average. This pressure equilibration typically takes several years and the onset of the reduction in the effectiveness of this production measure is currently observed. Production from these five clusters has currently ceased.

A more sophisticated computational scheme which minimizes a chosen measure of seismic risk across the field by finding an optimal distribution of a given total produced volume has also been developed.

SEISMOLOGICAL MODELS

The seismological models developed for the Groningen field (Bourne and Oates 2017, Bourne et al. 2018) include the joint conditional probability distributions of earthquake origin times, epicenters, and magnitudes given the reservoir deformations induced by pore-pressure decreases. Future reservoir pressure decreases are forecast using the reservoir fluid flow model for a given production schedule and assessment period. Reservoir pore pressure changes induce poro-elastic reservoir stress changes that govern the frictional stability of geological faults as measured by the Coulomb stress. The total Coulomb stress model depends on a stochastic model for the unresolved initial stress state of faults and a deterministic model for the resolved incremental Coulomb stresses induced by pore pressure depletion. Initial Coulomb stresses are treated stochastically as they depend on unresolved heterogeneities such as fault roughness and diagenesis. Incremental Coulomb stresses are treated deterministically as they depend on geometric and elastic heterogeneities resolved by reflection seismic imaging and geodetic monitoring, respectively.

Induced seismicity depends on the probability distribution of largest total Coulomb stresses and leads to an exponential-like increase in activity rates (Bourne and Oates 2017) and an inverse power-law-like decrease in *b*-values (Bourne et al. 2018). The distribution of maximum possible magnitudes used was proposed by a panel of experts after reviewing all the available data (Bommer and van Elk 2017). Aftershocks are included using the Epidemic Type Aftershock Sequence model (Bourne et al. 2018).

Bayesian inference is used to obtain the distribution of history-matched models given the observed history of reservoir pressure depletion, strain and induced seismicity. To evaluate forecast performance, the distribution of models obtained by history-matching observations from 1995 to 2012 are used to compute the likelihood of the observed seismicity from 2012 to 2017 given the model-based forecast for this same period. The results indicate that the best-performing seismological models yield pseudo-prospective forecasts[1] consistent with observations (Figure 8).

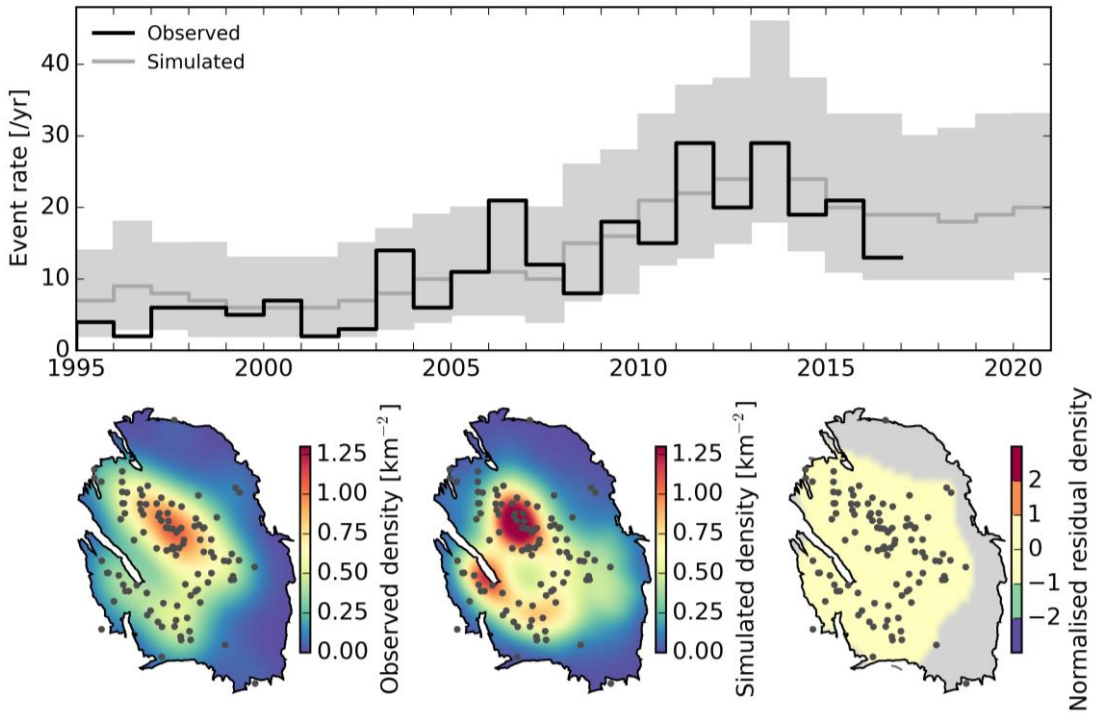

Figure 8. Temporal and spatial density of observed and simulated M≥1.5 events. Simulated temporal densities are represented by the median and the 95% prediction interval. Simulated spatial densities are represented as the median density map, and the normalized residuals relative to the observed density map where the 95% prediction interval corresponds to normalized residuals in the range -2 to 2.

[1] A pseudo-prospective forecast is made by splitting the observed earthquake catalogue into two separate time intervals. The first catalogue interval is used to condition the seismological model, and the second is used to evaluate its forecast performance. This contrasts with a prospective forecast that is made before the second time interval starts and then requires waiting for it to end.

These models include the effects of reservoir geometry, elastic stiffness, initial stress, and aftershocks on the spatial-temporal evolution of reservoir stress. Sensitivity tests with alternative simpler models all exhibit significantly lower forecast performance for the rates (Bourne & Oates 2017) and magnitudes (Bourne et al. 2018) of induced seismicity.

GROUND MOTION MODELS

In view of the shallow focus of the Groningen earthquakes, the travel paths to the surface that traverse the high-velocity Zechstein salt layer (Figure 3), and the thick layers of soft deposits at the surface, it was considered necessary from the outset to develop a locally calibrated ground-motion prediction model (Bommer et al. 2016). Source, path and site parameters for the reference rock horizon at 800 m depth were estimated from inversions of recorded motions and these were then used as input to finite-fault simulations of spectral accelerations (for periods from 0.01 to 5 s) and peak ground velocity for events from M_L 2.5 to greater than 7 (Edwards et al. 2018). The upper limit is determined by the Mmax distribution, whereas the lower limit of magnitude considered in the risk calculations depends on the desired risk metric, with lower values being more appropriate for damage estimation than those used for calculations in terms of casualties (Bommer and Crowley 2017). In order to accommodate the uncertainty associated with extrapolations from the upper limit of M_L 3.6 in the database to magnitudes in excess of M_L 7, the model includes four branches for the stress parameter (taking values of 75, 140, 220 and 300 bars for M_L 5 and greater, and values of 50, 70, 70 and 100 bars in the range of the Groningen data), with the uppermost branch designed to predict motions typical of tectonic earthquakes (Bommer et al. 2017a, 2017b).

The ground motions at the rock horizon at the base of the Lower North Sea formation are adjusted to the ground surface via nonlinear, frequency-dependent amplification factors defined for 160 zones over the field (Figure 9). For short oscillator periods, the linear portion of amplification factors was found to depend on magnitude and distance (Stafford et al. 2017), which is the cause of the dip in the spectra observed in Figure 9(b). The framework for the derivation of the ground-motion model, including the variability components and how the model both matches the Groningen data and captures epistemic uncertainty associated with extrapolation to larger magnitudes, is fully explained in Bommer et al. (2017a) and Bommer et al. (2017b).

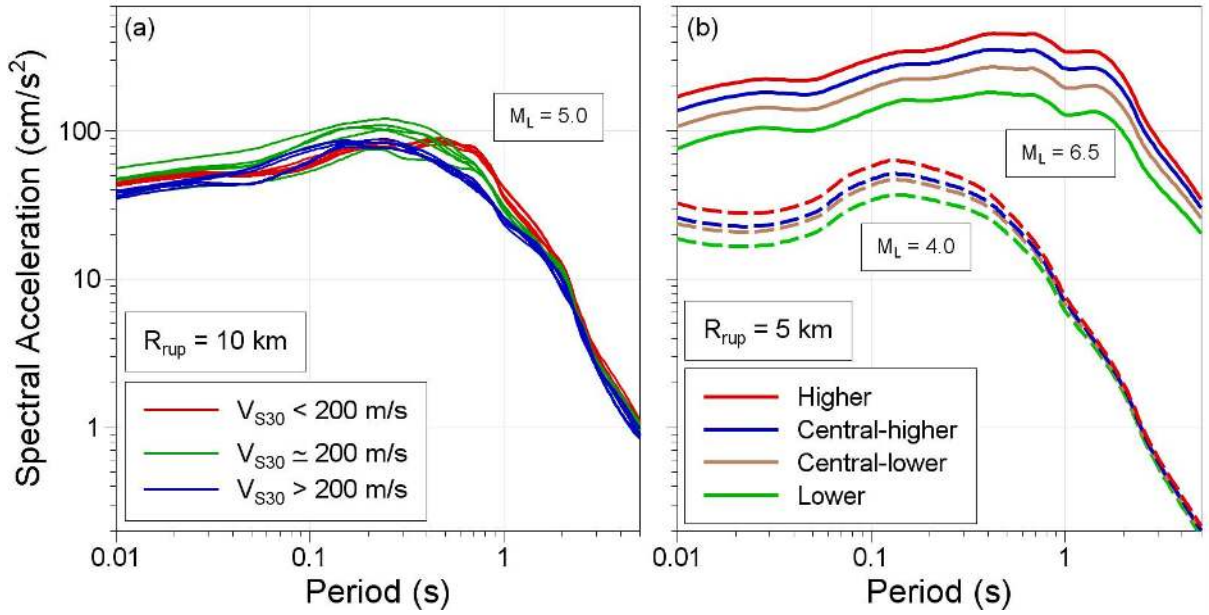

Figure 9. Predicted mean response spectra for (a) M_L 5, R_{rup} = 10 km, for 6 zones, covering the range of V_{S30} values in the field (the red and blue curves representing the stiffest and softest zones, respectively, and the green lines the zones with V_{S30} close to the field average of 200 m/s), using the lower-central branch of the logic tree, and (b) in one zone for two magnitudes and R_{rup} = 5 km, using all four logic-tree branches. The coefficients of the predictive model are applied without smoothing.

Since some of the fragility functions are defined in terms of both spectral accelerations and durations (significant durations based on 5-75% accumulation of Arias intensity), a model for the prediction of significant duration was also developed using the outputs from the simulations combined with V_{S30}-based amplification factors adapted from the model of Afshari and Stewart (2016). The duration model, which captures the very short (< 1 second) durations for ground motions at the epicenter observed for Groningen earthquakes and the rapid increase of the durations with distance, is presented in Bommer et al. (2017a). For applications in the risk model to groups of different buildings types at any given location, the model also includes a correlation matrix for the intensity measures (spectral accelerations at 23 periods and duration).

EXPOSURE MODELS

The building and population database described previously incorporates all known data about the buildings and their inhabitants in the Groningen area. However, the structural system (described in terms of structural material, lateral load-resisting system, and floor material) is only known for those buildings for which inspections have been carried out, or for which structural drawings have been collected. In order to assign a structural system to each building within the database, it has been necessary to infer this information from the

structural layout and the age of the building (Arup 2017c). These inference rules, which provide the likelihood of a range of structural systems given the layout and age, have been developed using the detailed structural data available from the inspections and drawings, as well as the expert judgment of local engineers, and are subject to continual validation as more information on inspected buildings within the region becomes available. The final exposure model is thus a probabilistic model that provides, for each unique building in the database, the probability of a range of structural systems. Figure 10 shows that once these percentages are summed across the field, the majority of the buildings in the region are constructed in unreinforced masonry (MUR).

The epistemic uncertainty in the exposure model has been explored by applying different inference rules, but it was not found to contribute significantly to the overall epistemic uncertainty in the risk results across the field, and is thus no longer modeled. Nevertheless, a significant effort is still being made to replace the probabilistic inference rules with inspection data, such that it will be possible to identify each individual building that needs structural upgrading as part of the mitigation plans.

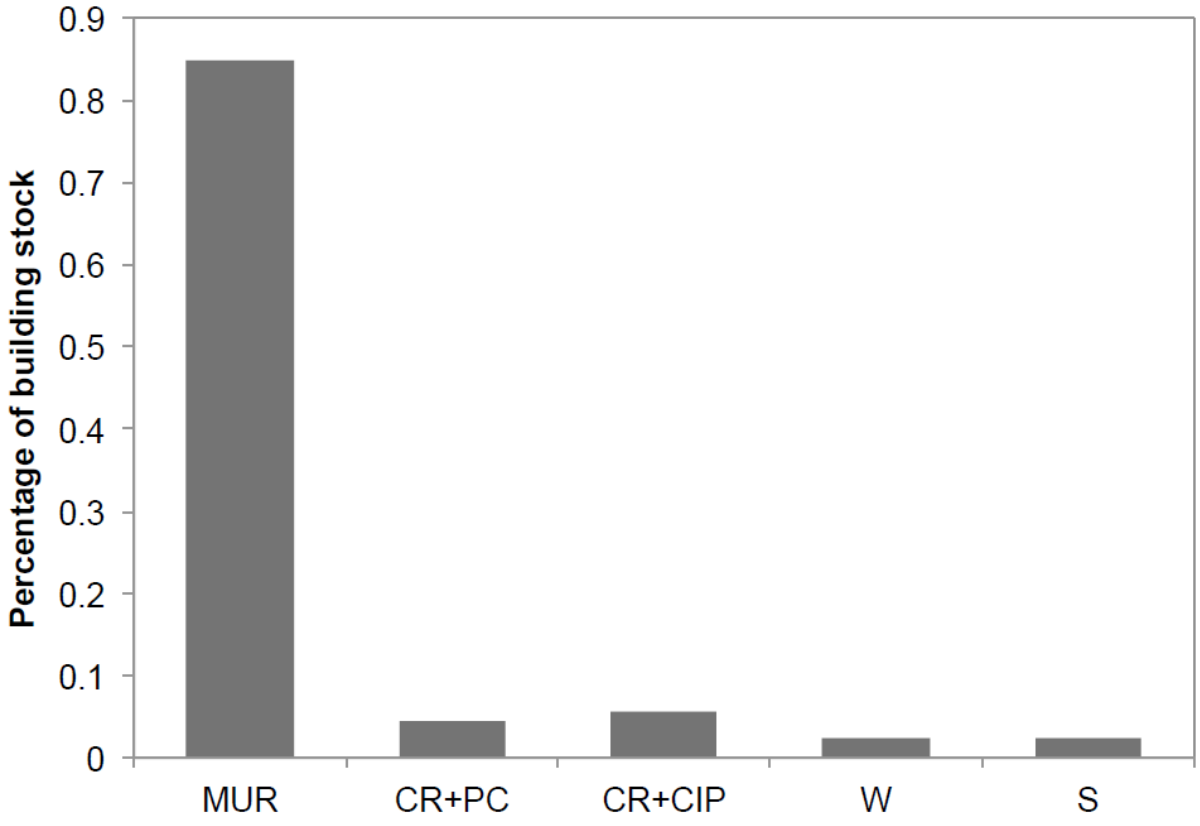

Figure 10. Percentage of each structural material used in the construction of occupied buildings in the region, where MUR = unreinforced masonry, CR+PC = precast reinforced concrete, CR+CIP = cast-in-place reinforced concrete, W = wood/timber, and S = steel.

FRAGILITY MODELS

As has been described previously, a large effort is being made to experimentally test a number of representative structural systems from the region and to develop calibrated numerical models. Nonlinear dynamic analyses of these calibrated models are undertaken to develop single-degree-of-freedom (SDOF) systems for the purposes of developing fragility models for each structural system (as fully described in Crowley et al. 2017 and Crowley et al. 2018). Two approaches have been taken to validate the SDOF systems: 1) a comparison of the estimated displacement responses of the SDOF and the MDOF models under the same set of records has been made, 2) the SDOF model has been used to blind predict the response of one of the latest shake-table tests on a full scale terraced house (Miglietta et al. 2018). Figure 11 compares the peak base shear and attic displacement response blind prediction using the SDOF model (up until collapse was predicted) with the peak values obtained from the experimental test, which was stopped when the specimen was very close to collapse.

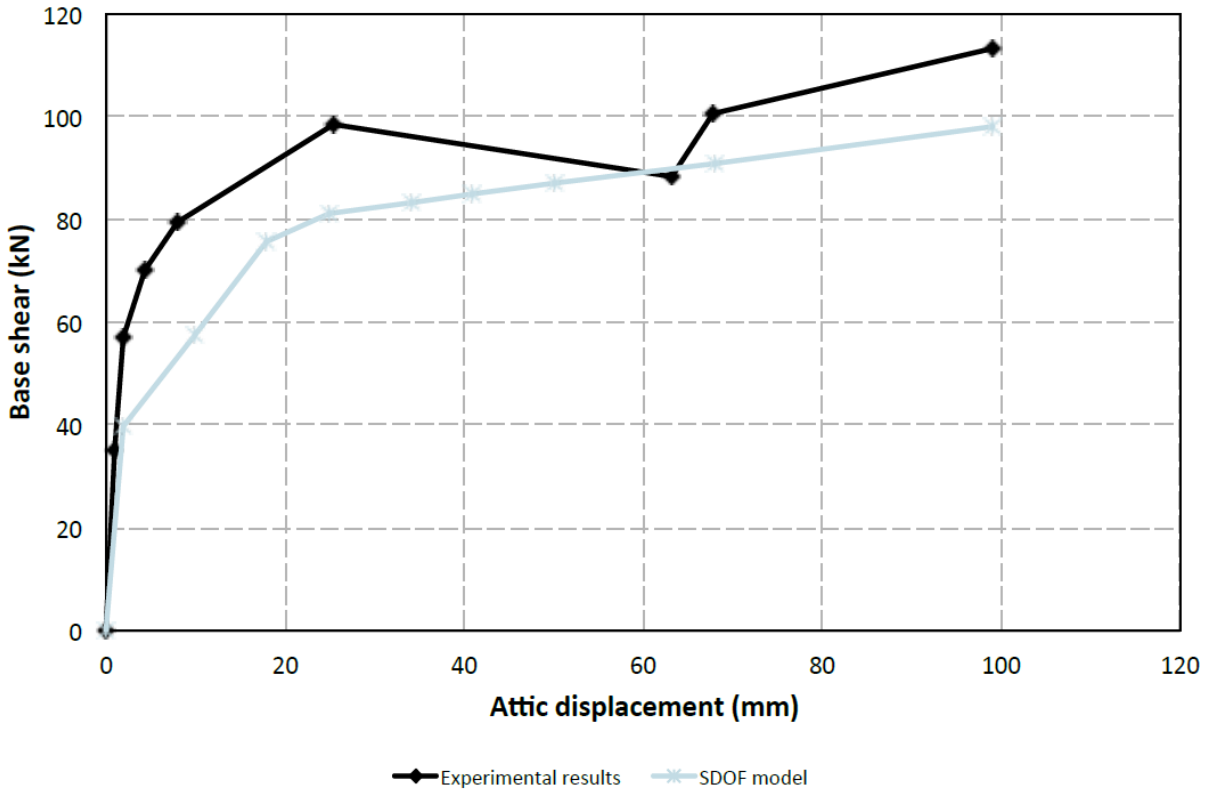

Figure 11. Comparison between the blind prediction, using the developed SDOF model, of the response of a full-scale terraced house specimen and the experimental shake table test results

The cloud method (Jalayer 2003, Cornell et al. 2002) has been employed for the development of fragility functions whereby multivariate linear regression of the displacement

response of the SDOF system to a large suite of records is undertaken. A number of different scalar and vector intensity measures have been considered, and the sufficiency (Luco and Cornell 2007) of each has been tested considering the magnitude, distance and a measure of strong ground shaking duration. Figure 12 shows example fragility functions where spectral acceleration at the fundamental period of vibration, $Sa(T_1)$, is a sufficient intensity measure.

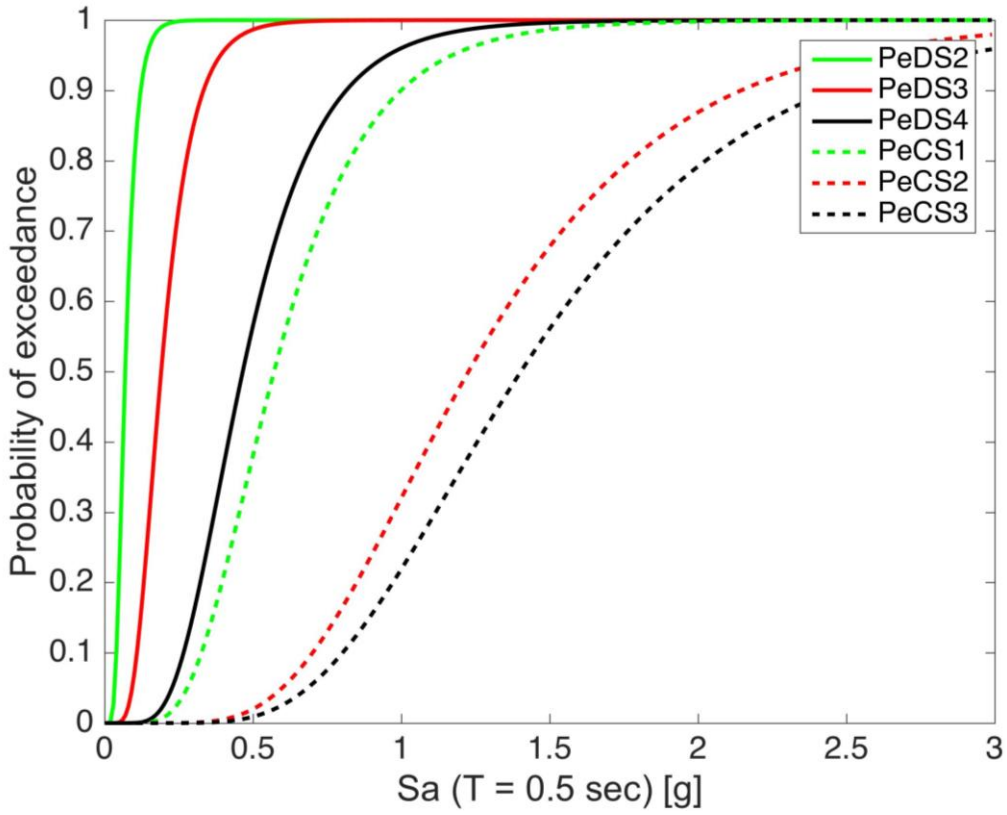

Figure 12. Set of fragility functions for one of the unreinforced masonry structural systems, where DS denotes the damage states and CS denotes the collapse states

For the masonry and reinforced concrete buildings, the displacement capacities for each damage state (from DS2 which refers to the initiation of structural damage to DS4 which refers to extensive structural damage) have been obtained from the experimental test campaign (see Graziotti et al. 2017b), whereas values from HAZUS (FEMA 2004) have been used for timber and steel structural systems that represent a limited number of mainly industrial/commercial buildings in the region. On the other hand, the displacement capacities for each collapse state (see examples of three collapse states in Figure 13, from CS1 that refers to floor collapse to CS3 which denotes global collapse of the structure) have been directly identified from the numerical modeling efforts described previously.

Figure 13. Collapse states observed in an unreinforced masonry numerical model during three different nonlinear dynamic analyses

Validation of the proposed damage fragility functions has been undertaken both through comparison with other European masonry fragility functions and through history checks, whereby the estimated number of damaged buildings due to the actual events with $M_L > 2.5$ that have been occurred in the field between 1995 and 2018 has been compared with the observed number of damaged buildings (see Crowley et al. 2018 for more details).

CONSEQUENCE MODELS

The consequences that are currently being modeled in the risk model include loss of life and damage. Crowley at el. (2017) present in detail the fatality model which relates the probability of loss of life to the extent of collapse of the buildings (obtained from the numerical models and experimental test results), together with a number of empirical coefficients proposed by Coburn and Spence (2002). The main causal pathways for loss of life that are currently being considered include the following: being hit by the collapse of a non-structural element (e.g. parapet or chimney) outside of the building, or being hit by the debris caused by partial or complete collapse of the building (both inside and outside). Damage, on the other hand, is predicted directly from the fragility functions presented previously.

RISK ESTIMATES AND SENSITIVITY CALCULATIONS

By way of illustration of the capacity of the Groningen seismic risk model, this section discusses some of the calculations that can be performed both to quantify the risk in different ways and to obtain insight into the factors exerting greatest influence on the risk.

COMPUTER CODE DEVELOPMENT AND VALIDATION

The Groningen risk model, which includes time-varying induced seismicity, lateral-varying site response characteristics over a region of some 1,000 km^2, and several tens of thousands of exposed buildings, is highly complex and the calculations using Monte-Carlo simulations include several innovative features. Convinced that it was therefore essential to apply rigorous quality control on both the algorithms and their application to the specific context of the Groningen field to ensure accurate risk estimation, two distinct computer codes with the same functionality were maintained and developed – one in Python and the other in C. This is somewhat similar to probabilistic seismic hazard analysis (PSHA) practice for critical facilities such as nuclear power plants, where it is generally a requirement that the hazard calculation codes undergo formal qualification. For example, in one nuclear project, the full logic-tree was implemented in two separate and previously qualified calculation codes (Bommer et al. 2013), but this was an exceptionally rigorous approach compared to standard practice. Throughout the development process and cycle of hazard and risk assessments, the outputs from these two codes were repeatedly compared against each other to validate our results (Figure 14).

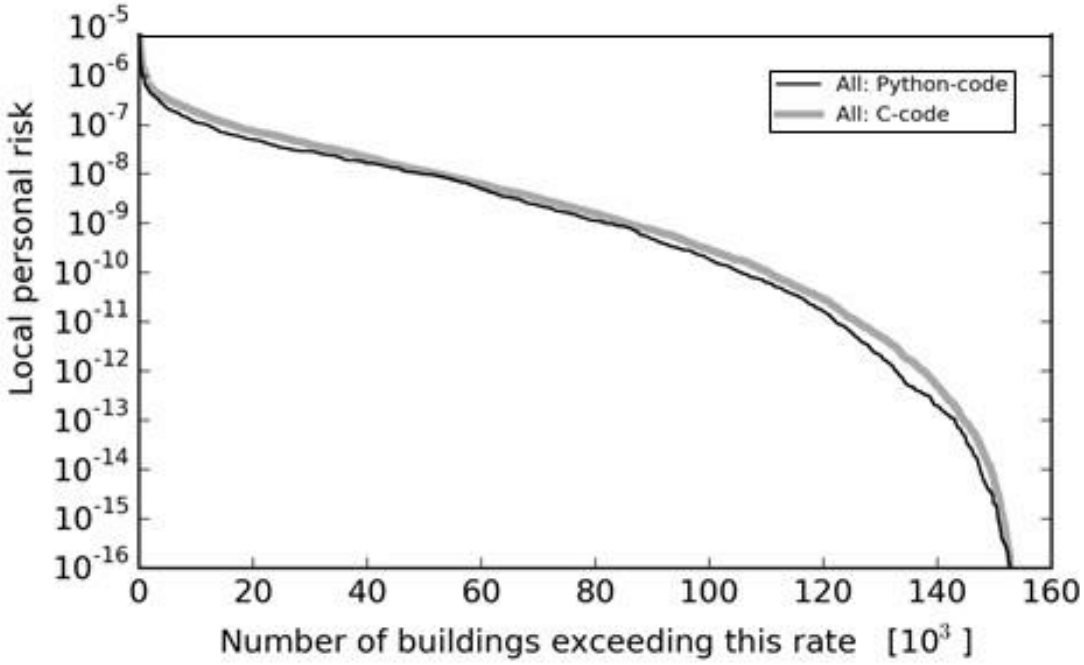

Figure 14. Example code benchmark plots of inside local personal risk (ILPR), for all building typologies, for the base case of the logic tree (Mmax=5.75; central branch of the GMM) for 27 bcm per year production from 2016-2021. Note the close agreement between C and Python results.

DISAGGREGATION

Disaggregation of the probabilistic seismic risk metrics obtained by Monte Carlo sampling provides a measure of the fractional contribution made by different elements within the risk model. In terms of the underlying hazard, the risk contributions from different magnitudes, M, distances, R, and ground motion residuals (i.e., the number, ε, of standard deviations, σ) are identified. Figure 15 shows disaggregation results obtained for M, R and ε.

The modal magnitude (i.e., the value of magnitude with the highest probability from the disaggregation distribution) for contributions to the LPR metric depends on location and building typology but is typically in the range $5.0 < M < 5.5$. Source-to-site distances less than 5 km contribute the most risk for buildings located within the center of the field where most of the seismicity occurs. Outside this region, the modal contribution increases with distance from the center up to 10 to 15 km. The modal contribution of ε also depends on location. Within the central area the largest risk contributions are from the interval $1.5 < \varepsilon < 2$, whereas outside this region the largest contributions are from larger epsilon values in the range $2 < \varepsilon < 3$.

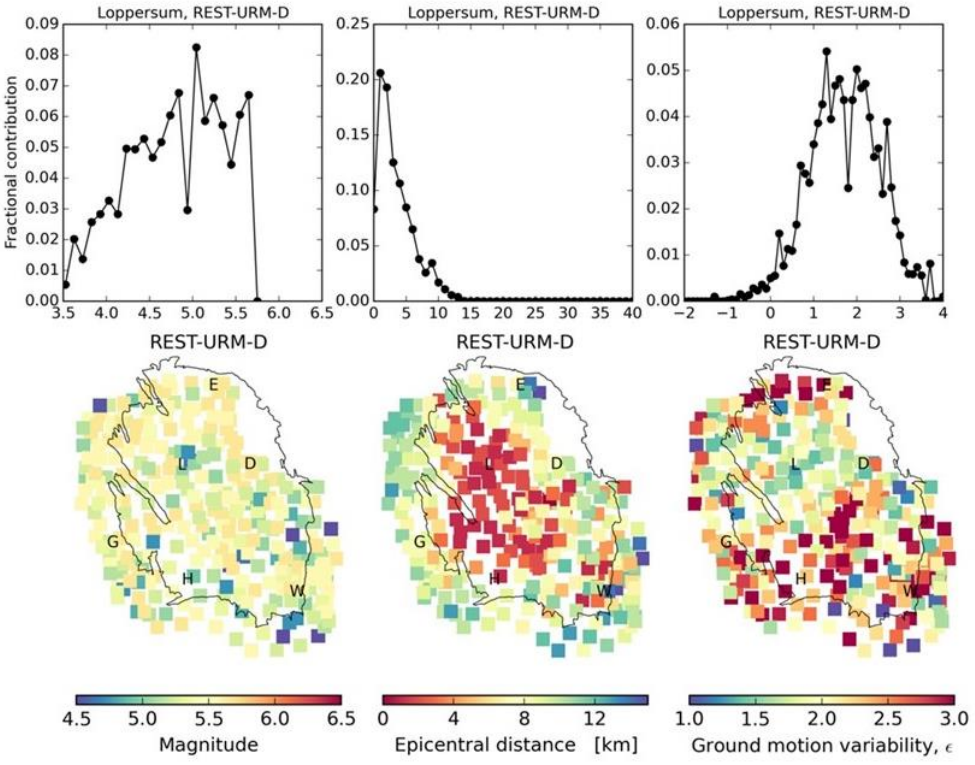

Figure 15. The fractional contribution of magnitude, epicentral distance, and ε to the ILPR for a selected typology (unreinforced masonry house) at selected location (Loppersum village) for the central branch of the logic tree (top) (see Figure 16). Maps to indicate spatial variation in the modal contributions (bottom).

RISK SENSITIVITY

Figure 16 shows the logic-tree structure used for the risk calculations together with a tornado plot indicating the sensitivity of the mean estimates of the LPR (averaged across all locations and all building the field, used as a convenient single measure of the risk for this purpose) to these different sources of epistemic uncertainty (by maintaining all branches for the nodes constant except for those corresponding to the one being explored, which are implemented individually with a weight of 1). The figure shows that the greatest contributor to the uncertainty on the risk estimates is the distribution on maximum magnitude, followed by the uncertainty associated with the fragility functions. The median ground-motion predictions are also an important source of epistemic uncertainty whereas the uncertainty on the variance in the GMM is a minor contributor, comparable to the uncertainty associated with the consequence model.

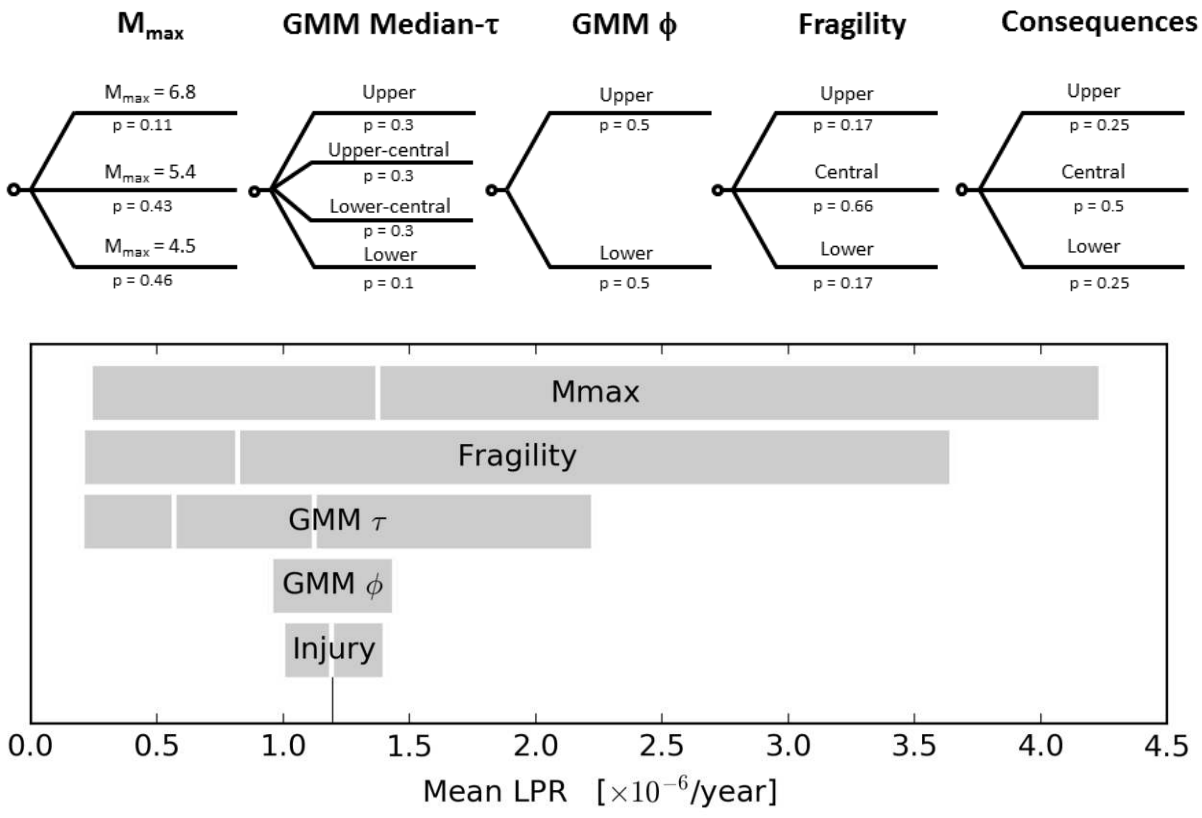

Figure 16. Logic-tree to characterize epistemic uncertainties (top), and the sensitivity of seismic risk to these epistemic uncertainties (bottom); the mean LPR values are calculated for a 24 bcm production scenario. GMM-τ indicates the median predictions of ground motions (and associated between-event variability) and GMM-ϕ the within-event variance in the ground-motion predictions.

622 The risk can be assessed for different production scenarios and then evaluated for
623 combinations of different measures to reduce seismic risk. Analysis of the risk assessments
624 prepared for the different production scenarios allows comparison of the effectiveness of
625 measures intended to achieve a reduction in the LPR and compliance with the safety norm.
626 In particular, the effectiveness of a reduction in the overall production from the field, the
627 optimization of the distribution of the offtake over the different areas of the field, and the
628 structural upgrading of buildings can be evaluated and compared. The number of buildings
629 not meeting the safety norm and the requirement to strengthen buildings is strongly
630 dependent on the production outlook for the Groningen field.

631 A reduction in the total production from the gas field will increase safety for all people
632 present in the Groningen field area. Both people exposed to a LPR above the safety norm of
633 10^{-5}/year and those exposed to a much lower seismic risk would have a risk benefit from a
634 reduction in production. The areal distribution of the field offtake can reduce risk for some
635 communities, but these effects are temporary, as the effect typically diminishes after several
636 years.

637 In contrast, structural upgrading of a building increases the safety of people present in or
638 around this particular building. Whereas a production reduction (for the full field or a field
639 area) effects the risk for all people in the area, structural upgrading is much more targeted to
640 the people in the selected building. Likewise, the other impacts of these measures to increase
641 safety are different for each community. A reduction of the overall production of the field is
642 primarily felt in the gas markets on a (inter)national level. The impact of building
643 strengthening of a house can be very substantial for the occupants.

644 The decision-making, balancing these options to reduce seismic risk for the Groningen
645 community, needs to be done by the Dutch Minister of Economic Affairs. Figure 16 shows
646 the results for a number of production scenarios developed by the pipeline transport company
647 responsible for security of supply to the gas markets. The gas volume produced during the
648 first 5 years (2018 – 2022) and the number of buildings that do not meet the safety norm are
649 shown for these scenarios. For a given gas production scenario, the plot thus shows the
650 number of buildings that would need to be strengthened to reduce the LPR to below the
651 thresholds of 10^{-4} and 10^{-5}. This plot also shows how instead of retrofitting the buildings a
652 choice could be made to reduce the gas production (i.e. moving from right to left in the plot)
653 and that mechanism could instead be used to reduce the number of buildings that exceed the

acceptable LPR threshold. This information could provide input for the comparison of the cost of retrofitting against the cost of reducing gas production.

DISCUSSION AND CONCLUSIONS

In this paper, the development and current status of a comprehensive seismic risk assessment model for the Groningen gas field has been presented Starting with gas production plans, the risk engine models the sequence of reservoir compaction, generation of induced and triggered earthquakes, ground shaking fields, structural damage and consequences for occupants. Epistemic uncertainty and aleatory variability associated with all elements of the model are incorporated into the risk calculations, so that either the mean risk or an appropriate fractile can be estimated. Illustrative examples have been shown of the capacity of the model to predict changes to the risk due to changes in gas production, building strengthening and combinations of both mitigation measures.

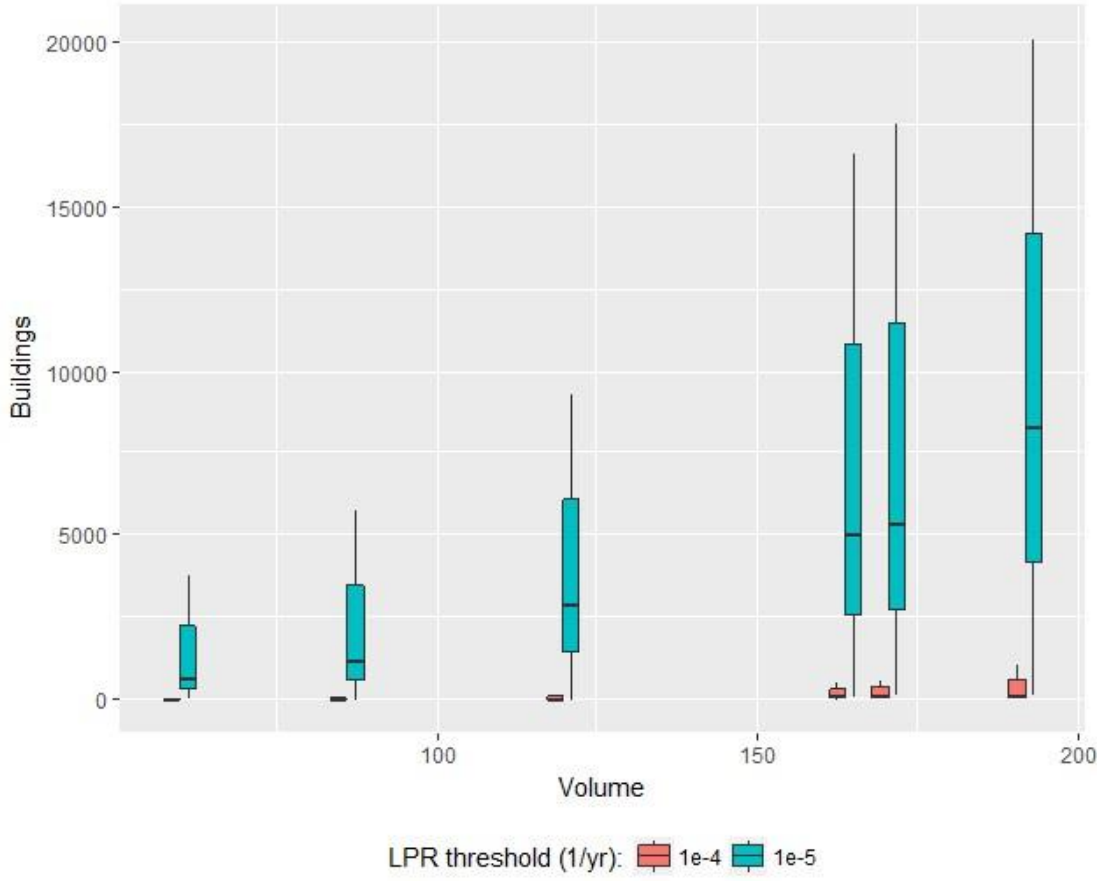

Figure 17. Box-whisker plot of the number of buildings in Groningen that do not meet the LPR-Norm for different production scenarios. On the horizontal axis the production volume [bcm] between 2018 and 2022 for the production scenario. In red the number of buildings with a LPR above 10^{-4}/year and in blue the number of buildings with a LPR above 10^{-5}/year. The boxes represent plus-and-minus one standard deviation and the lines indicate the minimum and maximum values.

Decision-making regarding appropriate risk mitigation measures will obviously also be influenced by numerous societal, political, economic and environmental considerations; the detailed discussion of such factors, whether in Groningen or more generally, are outside the scope of this paper. However, regardless of how much policy decisions are ultimately driven by such factors, we posit that it is essential to begin from an informed basis of quantitative risk estimates for different scenarios. The model developed for the estimation of induced seismic risk in the Groningen field may therefore provide a useful framework to be adapted to other cases of earthquakes generated by anthropogenic activities. The assessment of risk for different production scenarios demonstrates a combination of both production measures and building strengthening measures can be used to manage seismic risk.

ACKNOWLEDGMENTS

We thank both NAM and Shell for permission to publish this paper. The work presented in this paper has benefited from contributions from many individuals at NAM (especially Dirk Doornhof, Jeroen Uilenreef and Assaf Mar-Or, and also Remco Romijn for the cross-section of the field), and Shell Projects and Technology, as well as the seismologists at KNMI, particularly Bernard Dost. Other important contributions have come from Arup (for the exposure model development), Mosayk, TU Delft and Eucentre for structural analyses; Eucentre and LNEC for field and laboratory testing. We have also received valuable review and advice from many individuals, including Raphaël Steenbergen of TNO, Rien Herber of RUG, as well as SodM, the appointed Scientific Advisory Committee (SAC), and their international reviewers Stefan Wiemer, Stefan Baisch, and Iunio Iervolino for helpful feedback and challenge. Finally, we are grateful for the review comments from the Associated Editor, from Ivan Wong and from an anonymous reviewer, all of which help improved the clarity of the manuscript.

REFERENCES

Afshari, K., and Stewart, J. P., 2016. Physically parameterized prediction equations for significant duration in active crustal regions, *Earthquake Spectra* **32**(4), 2057-2081.

Arup, 2017a. *EDB V5 Data Documentation*, 229746_052.0_REP2005, November 2017. Available from URL: http://www.nam.nl/feiten-en-cijfers/onderzoeksrapporten.html

Arup, 2017b. Typology modelling: Analysis results in support of fragility functions - 2017 batch results, Report n. 229746_031.0_REP2005. November 2017. Available from URL: http://www.nam.nl/feiten-en- cijfers/onderzoeksrapporten.html

Arup, 2017c. EDB V5 post-analysis documentation, Report n. 229746_052.0_REP2018c, November 2017. Available from URL: http://www.nam.nl/feiten-en- cijfers/onderzoeksrapporten.html

Arup, TU Delft, Eucentre, 2015. *EUC-BUILD1: Modelling predictions and analysis cross validation. Report n. 229746_031.0_REP1004*. Available from URL: http://www.nam.nl/feiten-en-cijfers/onderzoeksrapporten.html

Arup, TU Delft, Eucentre and Arcadis, 2016. *EUC-BUILD2: Modelling predictions and analysis cross validation*, Report n. 229746_031.0_REP1009. Available from URL: http://www.nam.nl/feiten-en-cijfers/onderzoeksrapporten.html

Arup, TU Delft, Eucentre and Mosayk, 2017. *LNEC-BUILD1: Modelling predictions and analysis cross validation*, Report n. 229746_031.0_REP2004. Available from URL: http://www.nam.nl/feiten-en-cijfers/onderzoeksrapporten.html

Bommer, J. J., and Crowley, H., 2017. The purpose and definition of the minimum magnitude limit in PSHA calculations, *Seismological Research Letters* **88**(4), 1097-1106.

Bommer, J. J., and van Elk, J., 2017. Comment on "The maximum possible and the maximum expected earthquake magnitude for production-induced earthquakes at the gas field in Groningen, The Netherlands" by Gert Zöller and Matthias Holschneider, *Bulletin of the Seismological Society of America* **107**(3), 1564-1567.

Bommer, J.J., Strasser, F.O., Pagani, M., and Monelli, D., 2013. Quality assurance for logic-tree implementation in probabilistic seismic hazard analysis for nuclear applications: A practical example, *Seismological Research Letters* **86**(6), 938-945.

Bommer, J. J., Crowley, H., and Pinho, R., 2015. A risk-mitigation approach to the management of induced seismicity, *Journal of Seismology* **19**(2), 623-646.

Bommer, J. J., Dost, B., Edwards, B., Stafford, P. J., van Elk, J., Doornhof, D. and Ntinalexis, M., 2016. Developing an application-specific ground-motion model for induced seismicity, *Bulletin of the Seismological Society of America* **106**(1), 158-173.

Bommer, J. J., Stafford, P. J., Edwards, B., Bernard, D., van Dedem, E., Rodriguez-Marek, A., Kruiver, P., van Elk, J., Doornhof, D., and Ntinalexis, M., 2017a. Framework for a ground-motion model for induced seismic hazard and risk analysis in the Groningen gas field, The Netherlands, *Earthquake Spectra* **33**(2), 481-498.

Bommer, J.J., Dost, B., Edwards, B., Kruiver, P. P., Ntinalexis, M., Rodriguez-Marek, A., Stafford, P.J., and van Elk, J., 2017b. Developing a model for the prediction of ground motions due to earthquakes in the Groningen gas field. *Netherlands Journal of Geoscience* **96**(5), s203-s213.

Borsje, H., Pruiksma, J.P., and de Richemont, S.A.J., 2016. *Monitoring Network Building Vibrations - Analysis Earthquakes in 2014 and 2015*, TNO report TNO 2016 R11323/A, 12 December 2016.

738 Bourne, S. J., and Oates, S. J., 2017. Extreme threshold failures within a heterogeneous elastic thin-
739 sheet account for the spatial-temporal development of induced seismicity within the Groningen
740 gas field, *Journal of Geophysical Research: Solid Earth* **122**(12), 10299-10320.

741 Bourne, S. J., Oates, S. J., Bommer, J. J., Dost, B., van Elk, J., and Doornhof, D., 2015. A Monte
742 Carlo method for probabilistic seismic hazard assessment of induced seismicity due to
743 conventional gas production, *Bulletin of the Seismological Society of America* **105**(3), 1721-1738.

744 Bourne, S. J., Oates, S. J., and van Elk, J., 2018. The exponential rise of induced seismicity in the
745 Groningen gas field and its implications for controlling seismic risk. *Geophysical Journal*
746 *International* **213**, 1693-1700.

747 Bourne, S. J., Oates, S. J., van Elk, J., and Doornhof., D., 2014. A seismological model for
748 earthquakes induced by fluid extraction from a subsurface reservoir, *Journal of Geophysical*
749 *Research: Solid Earth* **119**(12), 8991-9015.

750 Brunesi, E., and Nascimbene, R., 2017. Experimental and numerical investigation of the seismic
751 response of precast wall connections, *Bulletin of Earthquake Engineering* **15**(12), 5511-5550.

752 Brunesi, E., Peloso, S., Pinho, R., Nascimbene, R. 2018a. Cyclic testing and analysis of a full-scale
753 cast-in-place reinforced concrete wall-slab-wall structure. *Bulletin of Earthquake Engineering*
754 **16**(10), 4761–4796.

755 Brunesi, E., Peloso, S., Pinho, R., Nascimbene, R. 2018b. Cyclic testing of a full-scale two-storey
756 reinforced precast concrete wall-slab-wall structure. *Bulletin of Earthquake Engineering* **16**(11),
757 5309–5339.

758 Coburn, A., and Spence, R., 2002. *Earthquake Protection*, 2nd Edition, John Wiley & Sons Ltd,
759 Chichester.

760 Cornell, A.C., Jalayer, F., Hamburger, R.O., 2002. Probabilistic basis for 2000 SAC Federal
761 Emergency Management Agency steel moment frame guidelines, *Journal of Structural*
762 *Engineering* **128**, 526–532.

763 Crowley, H., Polidoro, B., Pinho, R., and van Elk, J., 2017. Framework for developing fragility and
764 consequence models for local personal risk, *Earthquake Spectra* **33**(4), 1325-1345.

765 Crowley, H., Pinho, R., van Elk, J., and Uilenreef, J., 2018. Probabilistic damage assessment of
766 buildings due to induced seismicity, *Bulletin of Earthquake Engineering*,
767 https://doi.org/10.1007/s10518-018-0462-1.

768 Cvetkovich, G, and Löfstedt, 1999, R., Social Trust and the Management of Risk, Earthscan, ISBN
769 978-1-85383-604-6.

Dost, B., Edwards, B., and Bommer, J. J., 2018. The relationship between **M** and M_L - a review and application to induced seismicity in the Groningen gas field, the Netherlands, *Seismological Research Letters,* **89**(3), 1062-1074.

Dost, B., Goutbeek, F., van Eck, T., and Kraaijpoel, D., 2012. Monitoring induced seismicity in the North of the Netherlands: status report 2010, *KNMI Scientific report WR 2012-03*.

Dost, B., Ruigrok, E., and Spetzler, J., 2018a. Development of probabilistic seismic hazard assessment for the Groningen gas field, *Netherlands Journal of Geoscience* **96**(5), s235-s245.

Douglas, J., and Aochi, H., 2014. Using estimated risk to develop stimulation strategies for enhanced geothermal systems, *Pure and Applied Geophysics* **171**, 1847-1858.

Edwards, B., Zurek, B., van Dedem, E., Stafford, P. J., Oates, S., van Elk, J., deMartin, B., ~~and~~ Bommer, J. J., 2018. Simulations for the development of a ground motion model for induced seismicity in the Groningen gas field, The Netherlands. Bulletin of Earthquake Engineering, https://doi.org/10.1007/s10518-018-0479-5.

FEMA (2004). *HAZUS-MH Technical Manual*. Federal Emergency Management Agency, Washington D.C.

Graziotti, F., Rossi, A., Mandirola, M., Penna, A., Magenes, G., 2016a. Experimental characterization of calcium-silicate brick masonry for seismic assessment. *Proceedings of the 16th International Brick and Block Masonry Conference (IBMAC)*, Padua, Italy, 1619-1627.

Graziotti, F., Tomassetti, U., Penna, A., and Magenes, G., 2016b. Out-of-plane shaking table tests on URM single leaf and cavity walls. *Engineering Structures* **125**, 455-470.

Graziotti, F., Tomassetti, U., Kallioras, S., Penna, A., Magenes, G., 2017a. Shaking table test on a full scale URM cavity wall building. *Bulletin of Earthquake Engineering* **15**(12), 5329–5364.

Graziotti, F., Tomassetti, U., Penna, A., Magenes, G., 2017b. *Tests on URM clay and calcium-silicate masonry structures: identification of damage states*. Eucentre Foundation, Pavia, Italy. Working Version of October 2017. Available from URL: http://www.nam.nl/feiten-en-cijfers/onderzoeksrapporten.html

Graziotti, F., Tomassetti, U., Sharma, S., Grottoli, L., Magenes, G., 2018a. Experimental response of URM single leaf and cavity walls in out-of-plane two-way bending generated by seismic excitation. *Construction Building Materials*, https://doi.org/10.1016/j.conbuildmat.2018.10.076.

Graziotti, F., Penna, A., Magenes, G., 2018b. A comprehensive in-situ and laboratory testing programme supporting seismic risk analysis of URM buildings subjected to induced earthquakes. *Bulletin of Earthquake Engineering*, https://doi.org/10.1007/s10518-018-0478-6.

Harris, C., and Bourne, S. J., 2017. Computing the distribution of Pareto sums using Laplace Transformation and Stehfest inversion, *Pure and Applied Geophysics* **174**(5), 2039-2075.

Houtgast, G, 1992. *Catalogus Aardbevingen in Nederland*, KNMI Publication 179. 2nd edition.

Hunfeld, L. B., Niemeijer, A. R., Spiers, C. J. (2017). Frictional properties of simulated fault gouges from the seismogenic Groningen gas field under in situ P–T chemical conditions. *Journal of Geophysical Research: Solid Earth*, **122**. https://doi.org/10.1002/2017JB014876

Jalayer, F. 2003. *Direct probabilistic seismic analysis: Implementing non-linear dynamic assessments*, *Ph.D. Dissertation*, Stanford University.

Kallioras, S., Guerrini, G., Tomassetti, U., Marchesi, B., Penna, A., Graziotti, F., Magenes, G. 2018. Experimental seismic performance of a full-scale unreinforced clay-masonry building with flexible timber diaphragms. *Engineering Structures* **161**, 231-249.

Ketelaar, V. B. H., 2008. *Monitoring Surface Deformation Induced by Hydrocarbon Production Using Satellite Radar Interferometry*, TUD Technische Universiteit Delft, Delft, the Netherlands.

Ketelaar, V. B. H., 2009. *Satellite Radar Interferometery: Subsidence Monitoring Techniques*, Springer Science + Business Media.

KNMI, 2017. *Koninklijk Nederlands Meteorologisch Instituut Seismic and Acoustic Data Portal.* http://rdsa.knmi.nl/dataportal/

Kruiver, P. P., van Dedem, E., Romijn, R., de Lange, G., Korff, M., Stafleu, J., Gunnink., J. L., Rodriguez-Marek, A., Bommer, J. J., van Elk, J., and Doornhof, D., 2017. An integrated shear-wave velocity model for the Groningen gas field, The Netherlands, *Bulletin of Earthquake Engineering* **15**(9), 3555-3580.

Luco, N., and Cornell, C.A., 2007. Structure-specific scalar intensity measures for near-source and ordinary earthquake ground motions, *Earthquake Spectra*, **23**(2), 357-392.

Majer, E. L., Baria, R., Stark, M., Oates, S., Bommer, J., Smith B., and Asanuma, H., 2007. Induced seismicity associated with Enhanced Geothermal Systems, *Geothermics* **36**, 185-222.

Majer, E., Nelson, J., Robertson-Tait, A., Savy, J., and Wong, I., 2012. *Protocol for Addressing Induced Seismicity Associated with Enhanced Geothermal Systems*. DOE/EE-0662, US Department of Energy.

Malomo, D., Pinho, R., and Penna A., 2017. Modelling the in-plane behaviour of URM walls by the Applied Element Method, *Earthquake Engineering and Structural Dynamics* **47**, 1610–1630.

Miglietta, M., Mazzella, L., Grottoli, L., Guerrini, G., Graziotti, F., 2018. *Shaking table test of a full-scale cavity-wall terraced house specimen representative of the Groningen building stock*. Report n. EUC160/2018U, Eucentre, Pavia, Italy.

Mignan, A., Landtwing, D., Mena, B., and Wiemer, S., 2015. Induced seismicity risk assessment for the 2006 Basel, Switzerland, enhanced geothermal system project: role of parameter uncertainty on risk mitigation, *Geothermics* **53**, 133-146.

838 Mosayk, 2017. *Nonlinear dynamic analysis of index buildings for v5 fragility and consequence*
839 *models*, Report n. D8. Available from URL: http://www.nam.nl/feiten-en-
840 cijfers/onderzoeksrapporten.html

841 Noorlandt, R. P., Kruiver, P. P., de Kleibe, M. P. E., Karaoulis, M., de Lange, G., Di Matteo, A., von
842 Ketelhodt, J., Ruigrok, E., Edwards, B., Rodriguez-Marek, A., Bommer, J. J., van Elk, J., and
843 Doornhof, D., 2018. Characterisation of ground-motion recording stations in the Groningen gas
844 field, *Journal of Seismology* **22**(3), 605–623.

845 Pijnenburg, R. P. J., Verberne, B. A., Hangx S. J. T. and. Spiers, C. J. (2018). Deformation behaviour
846 of sandstones from the seismogenic Groningen gas field: Role of inelastic versus elastic
847 mechanisms **123**(7), 5532-5558.

848 Rodriguez-Marek, A., Kruiver, P. P., Meijers, P., Bommer, J. J., van Elk, J., and Doornhof, D., 2017.
849 A regional site-response model for the Groningen gas field, *Bulletin of the Seismological Society*
850 *of America* **107**(5), 2067-2077.

851 Siegrist,M., Earle, T,C. and Gutscher, H., *Trust in Risk Management, Uncertainty and Scepticism in*
852 *the Public Mind*, Earthscan, ISBN 978- 1-84407-424-2.

853 Slovic, P., 2000, *The Perception of Risk – Risk Society and Policy Series*, Earthscan, ISBN 978-1-
854 84791-148-7

855 Slovic, P., 2010, *The Feeling of Risk – New perspectives on Risk Perception*, Earthscan, ISBN 978-1-
856 85383-528-5

857 Spetzler, J. and Dost, B., 2017. Hypocentre estimation of induced earthquakes in Groningen,
858 *Geophysical Journal International* **209**, 453-465.

859 Spica, Z. J., Perton, M., Nakata, N., Liu, X., and Beroza, G. C., 2018. Site characterization at
860 Groningen gas field area through joint surface-borehole H/V analysis, *Geophysical Journal*
861 *International,* **212**(1), 412–421.

862 Spiers, C.J., Hangx, S.J.T, and Niemeijer, A.R. (2017). New approaches in experimental research on
863 rock and fault behaviour in the Groningen gas field. *Netherlands Journal of Geosciences*, **96**(S5)
864 55-69.

865 Stafford, P. J., Rodriguez-Marek, A., Edwards, B., Kruiver, P. P., and Bommer, J. J., 2017. Scenario
866 dependence of linear site effect factors for short-period response spectral ordinates, *Bulletin of the*
867 *Seismological Society of America* 1**07**(6), 2859-2872.

868 Stafford, P. J., Zurek, B. D., Ntinalexis, M., and Bommer, J. J. 2018. Extensions to the Groningen
869 ground-motion model for seismic risk calculations: component-to-component variability and
870 spatial correlation, *Bulletin of Earthquake Engineering*, https://doi.org/10.1007/s10518-018-0425-
871 6.

van Oeveren, H., Valvatne, P., Geurtsen, L., and van Elk, J. 2017. History Match of the Groningen field dynamic reservoir model to subsidence data and conventional subsurface data, *Netherlands Journal of Geosciences* **96**(5), s47-s54.

Zoback, M. D., 2012. Managing the seismic risk posed by waste water disposal, *EARTH Magazine* **57**(4), American Geosciences Institute.